sustainability

MDPI

Article

Design and Optimization of Fractional Order PID Controller to Enhance Energy Storage System Contribution for Damping Low-Frequency Oscillation in Power Systems Integrated with High Penetration of Renewable Sources

Hasan Ali Abumeteir * and Ahmet Mete Vural

Electrical and Electronics Engineering Department, Gaziantep University, Sehitkamil, Gaziantep 27410, Turkey; mvural@gantep.edu.tr

* Correspondence: hmeteir@gmail.com

Abstract: This paper proposes adding a controller to the energy storage system (ESS) to enhance their contribution for damping low-frequency oscillation (LFO) in power systems integrated with high penetration of different types of renewable energy sources (RES). For instance, wind turbines and photovoltaic (PV) solar systems. This work proposes superconducting magnetic energy storage (SMES) as an ESS. The proportional–integral–derivative (PID) and fractional-order PID (FOPID) are suggested as supporter controllers with SMES. The PID and FOPID controller's optimal values will be obtained using particle swarm optimization (PSO) is used as the optimization method. Both local area and inter-area oscillation is considered in this work as a LFO. To investigate the impact of adding the SMES with the proposed controller, a multimachine power system with different integration scenarios and cases is carried out with a PV system and wind turbine. The system responses are presented and discussed to show the superiority of the proposed controller both in the time domain and by eigenvalues analysis.

Keywords: damping low-frequency oscillations; renewable energy sources; superconducting magnetic energy storage; particle swarm optimization; fractional-order; proportional–integral–derivative

Citation: Abumeteir, H.A.; Vural, A.M. Design and Optimization of Fractional Order PID Controller to Enhance Energy Storage System Contribution for Damping Low-Frequency Oscillation in Power Systems Integrated with High Penetration of Renewable Sources. *Sustainability* **2022**, *14*, 5095. https://doi.org/10.3390/su14095095

Academic Editors: Emad M. Ahmed, Mokhtar Aly and Fernanda Carnielutti

Received: 15 March 2022
Accepted: 21 April 2022
Published: 23 April 2022

1. Introduction

Globally, fears are increasing due to the increase in global warming resulting from power plants based on fossil fuels, and this appears in the form of a severe increase in temperatures. Furthermore, the global trend to confront global warming has produced energy from natural sources such as wind and the sun [1]. There is a continuous increase in investments and growing the capacity of renewable energy sources (RES), especially those that depend on wind and solar photovoltaic (PV) systems, as shown in Figure 1. The countries are looking to increase reliance on it as a major source of energy production to achieve sustainable development goals [2].

Although RES is considered environmentally friendly, there are several limitations of their utilization, such as low total inertia and fault ride, uncertainties due to climate conditions, voltage and frequency oscillations, and poor stability [3,4]. Providing the stability of power systems has been investigated as a challenge for secure operation since the 1920s [5]. Low-frequency oscillation (LFO) is the prime hazard limiting the stability of the power system [5]. The main reasons that lead to the LFOs are:

(1) lack of transmission line system,
(2) disparity between loads and generation units, and
(3) fluctuations in the load [6]. This paper considers two types of LFO: local area and inter-area oscillations. The inter-area oscillation mode was distinguished in the inefficient transmission systems linked to large generation units [6]. The inter-area oscillations

occur between [0.1–0.7] Hz. In contrast, the local area oscillation was notable in one of the generators in the power systems. The local area oscillation is between (0.7–2.0] Hz [5–8].

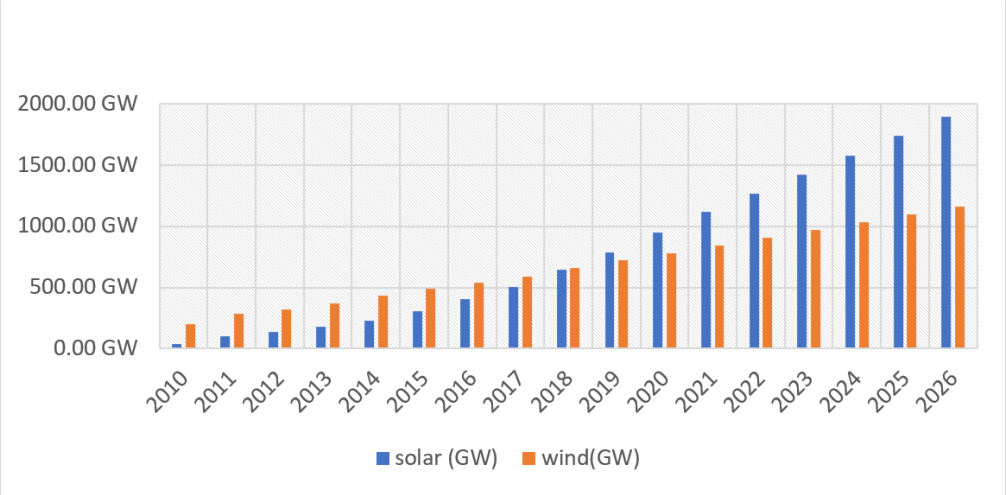

Figure 1. Cumulative Capacity of RES 2010–2026 [2].

Many related works are interested in studying the contribution of ESSs to enhance the damping LFO in the power systems due to the low prices and increased energy market investment worldwide. For instance, the authors in this work [9] proposed two optimization methods to select the best parameters for a different type of ESS to enhance the LFO mitigation in the two-area power system only without adding RES to the power grid. They used particle swarm optimization (PSO) and heuristic optimization methods based on supercapacitors and flywheels ESS. The impact of the battery system in a power system LFO and modal interaction with high penetration of RESs have been investigated in this work [10]. The gain variation of a battery controller has significantly affected the oscillation mode of the synchronous generators and modes coming from RES. The rated power contributed by the battery system has no effective impact on the various oscillation modes. The location of the battery system has an effective impact on the damping of the modes has been concluded [10]. The authors of this work [11] suggested designing an adaptive power oscillation damping controller for a static synchronous compensator with ESS to improve the damping LFO in the power system. The work has not considered RES in the study. The battery ESS was proposed in this work [11] for damping LFO in single and multi-machine power systems without considering the RES effects. A lead-lag droop-type controlled battery system with a recovery strategy state-of-charge is proposed in this work [12] to enhance the damping frequency response of the system with a high PV systems penetration in the power system only without considering the wind turbine. The wide area of power oscillation damping is proposed in this work [13] to increase the power system's resilience integrated with high-level RES. The optimization method used to obtain the optimal values of the controller was the differential evolution method. This work has not used any ESS. In the other work, the wide area was used with a multi-mode controller integrated with the battery system to increase the power system stability. The optimization method used to obtain the optimal values of the controller was the bat algorithm [14]. The general model of ESS is used with wide area control for damping inter-area oscillation in the multimachine power system only without RES integration [15]. The ultracapacitor energy storage is used for damping inter-area oscillation only without considering the local area oscillation in the multimachine power systems; in this work, no optimization method is used nor studying the effect of adding RES [16]. The wide area FOPID controller is used for damping inter-area LFO. The parameters of the controller are tuned by using differential evolution proposed for the multimachine power system in this work [17]. The different types of ESSs

are used [6]. The ultracapacitor and battery are two types of ESSs were used with a high penetration level of PV with multimachine power systems. The modeling and analysis of small-signal stability of power systems integrated with the high level of RES with the general model of ESSs are carried out in this work [18]. The integer mixed PSO method is used to get the optimal control and placement parameters of various battery energy units to enhance oscillation damping in a transmission power system [19].

The above literature works noted that different methods in the power system enhance the damping of LFO. Nevertheless, the energy systems associated with RES and ESS and how they can improve damping LFO were not presented. Thus, the importance of this work comes from different aspects:

(1) the integration between the multimachine power system and high penetration of RES is considered,
(2) adding SMES to the power system integrated with high penetration of RES such as wind turbine and PV solar system, and
(3) proposed a PSO to tune a PID and FOPID controllers to enhance the SMES contribution for damping LFO.

The organization of the paper is as follows: After this introduction, Section 2 presents the dynamic modeling of the studied power system. Section 3 describes the modeling of the PV system as well as the wind turbine. Section 4 provides the dynamical model of SMES. The mathematical implementation of PID and FOPID controllers are presented in Section 5. Section 6 describes the PSO method by defining the system's objective function. Section 7 presents the case studies of the suggested model. Section 8 shows the simulation results in time-domain and eigenvalues analysis. Finally, the conclusion is given in Section 9.

2. Power System Modeling

The dynamic differential equations are used to describe the power system for LFO studying. All generators have been implemented in the D-Q form, and a third-order model is considered. The power system consists of multiple areas; similar components are a synchronous generator, exciter, governor, and turbine [20].

2.1. Synchronous Generator

The third-order model represents all n generators [21]. The set of differential equations are presented as in Equations (1) and (2):

$$\Delta \dot{x} = A\Delta x + Bu \tag{1}$$

$$\Delta y = C\Delta x \tag{2}$$

where A is a $(n \times n)$, B is a $(n \times m)$, u is (mx1), and $x = \left[\omega, \delta, E'_q\right]$, and u respectively represent the vectors of state variables control variables. The detailed dynamic equations of a multimachine power system are given as follows:

$$\begin{cases} \dot{\delta}_n = \omega_n - \omega_0 \\ \dot{\omega}_n = \frac{\omega_0}{2H_n}(P_{mn} + P_{en} \pm P_{RESn} \pm P_{SMESn} - D_n\omega_0^{-1}(\omega_n - \omega_0)) \\ \dot{E}'_{qn} = T_{don}^{-1}(u_{fdn} + E_{fdn} - E_{qn}), n = 1, \ldots n \end{cases} \tag{3}$$

$$E_{qn} = x_{dn}I_{fn} = E'_{qn} + \left(x_{dn} - x'_{dn}\right)I_{dn} \tag{4}$$

$$\begin{cases} P_{en} = \sum_{j=1}^{n} E'_{qn}E'_{qj}\beta_{nj} \end{cases} \tag{5}$$

$$\begin{aligned} I_{dn} &= \sum_{j=1}^{n} E'_{qj}\alpha_{nj} \\ I_{qn} &= \sum_{j=1}^{n} E'_{qj}\beta_{nj} \end{aligned} \tag{6}$$

$$\begin{cases} V_{tn} = (V_{dn}^2 + V_{qn}^2)^{\frac{1}{2}} \\ V_{dn} = x_{qn} I_{qn} \\ V_{dn} = E'_{qn} - x'_{dn} I_{dn} \end{cases} \tag{7}$$

$$\begin{cases} \alpha_{ij} = B_{ij}\cos(\delta_i - \delta_j) + G_{ij}\sin(\delta_i - \delta_j) \\ \beta_{ij} = B_{ij}\sin(\delta_i - \delta_j) + G_{ij}\cos(\delta_i - \delta_j) \end{cases} \tag{8}$$

The n represents n^{th} generator; the rotor angle is represented by δ_n, and ω_n is represented the rotor speed of each generator, and ω_0 refers to synchronous speed. E_{0i}, and E_{qi} refers to the transient and synchronous q-axis voltage; E_{fdn} represents the filed voltage; P_{ei} and P_{mi} refer to the electric and mechanical power; V_{tn} donates the terminal voltage; V_{dn} and V_{qn} refer to the d–q axis terminal voltage; x_{dn} and x_{don} represent the synchronous and transient d-axis impedance; H_n represents the inertia of the rotor generator; D_n refers to the constant of the damping; T_{don} represents the d-axis transient time constant; I_{dn} and I_{qn} represent d–q axis current [22–24]. The P_{RESn} represents real power comes from PV, wind turbine units, or both. The P_{SMESn} represents the real power comes from SMES [25–28].

2.2. Governor System

The main function of the governor system in the synchronous generator is to control the torque magnitude delivered to the synchronous generator. The oscillation in the mechanical torque comes from the variation of generator speed or a change in the load. The governor system representing mathematically, as shown in Equation (9)

$$P_m = -\left[\frac{k_g}{1 + T_g s}\right]\omega_d \tag{9}$$

where k_g is gain constant, T_g refers to the governor time delay, and GSC is a grid side converter [13,23,24].

The block diagram of the governor system is illustrated in Figure 2.

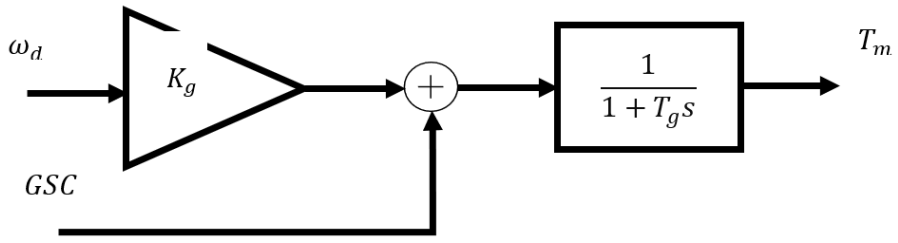

Figure 2. Governor system.

2.3. Excitation System

The excitation system is responsible for injecting a direct current (DC) into the rotor field winding to produce a magnetic field to excite the synchronous generator [23,24]. The transfer function given by Equation (10) of the excitation system is shown in Figure 3.

$$E_{fd} = \frac{K_{An}\left(V_t - V_{ref}\right)}{1 - T_{An} s} \tag{10}$$

where T_{An} is the exciter time delay, and K_{An} is gain constant.

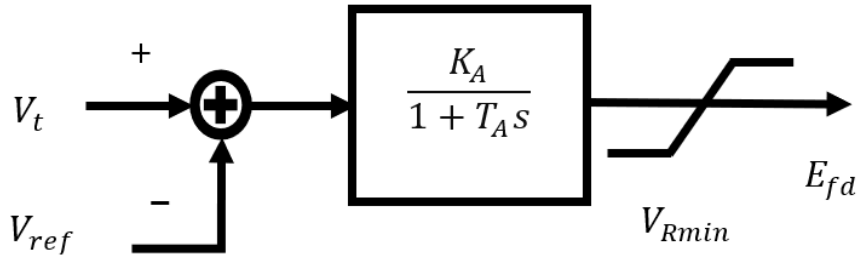

Figure 3. Excitation system.

3. RES Modeling

In this work, two types of RES will be used to integrate with the power system. The double fed induction generator (DFIG) and PV solar system are considered RES. The dynamic model will be presented to study the LFO of the power system with RES [13]. As the RESs generate power fickle nature, RES's powers variable [3]. Therefore, to reflect the sensible nature of RES, white noise is considered with the wind and PV system model [26].

3.1. PV

The PV system combines multiple PV arrays to produce power under solar irradiance. Every PV array is linked to the DC/DC converter, as shown in Figure 4. The output of every converter is linked to a common DC bus [29].

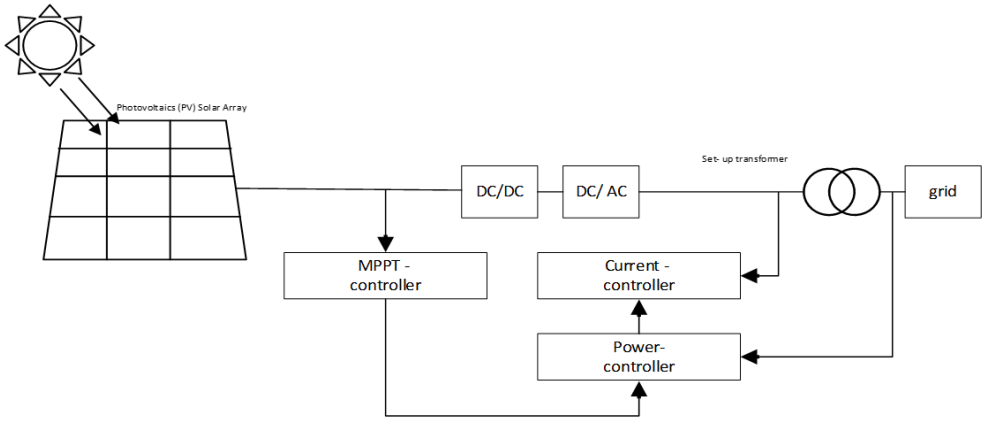

Figure 4. Model of PV system.

Maximum power point trackers control the converters. The total power of the PV system can be expressed in Equation (11):

$$P_{\mathrm{PV}} = \eta S \phi [1 - 0.005(T_a + 25)] \tag{11}$$

η refers to PV efficiency (%), S donates area (m^2), which are fixed for panels, ϕ and T_a represents solar insolation (kW/m^2) and ambient temperature (°C). The power mainly depends on ϕ and T_a [29].

3.2. Wind Turbine

The wind turbine is modeled as a single equivalent generator at a single substation for steady-state and dynamic analyses. The wind generators within the farm are collected by one group having an MV rating equal to the sum of ratings of all the units. Figure 5 shows the structure of DFIG integration to the power system. The stator and rotor flux dynamics of the DFIG are rapid compared to the grid dynamics [30].

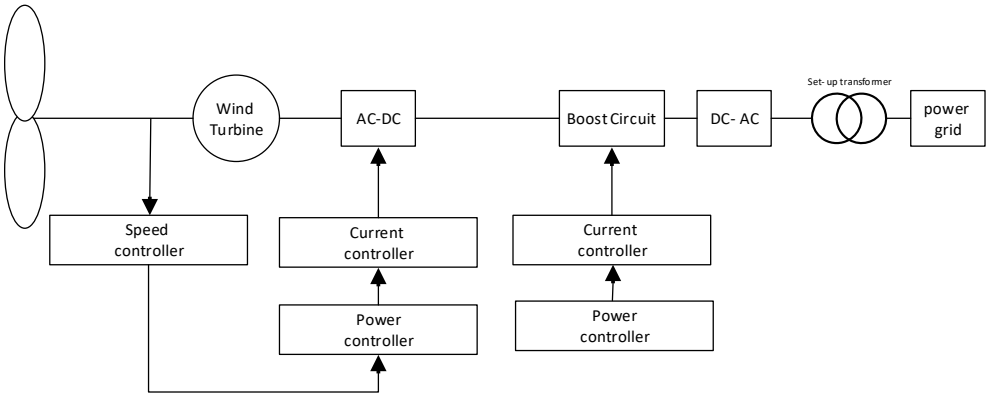

Figure 5. Model of wind turbine.

The power injected by DFIG into the power system is given:

$$P_{WT} = \frac{x_m}{x_m + x_s} v_i i_{rq} \tag{12}$$

where x_m is magnetization reactance, x_s is stator reactance, v_i is the voltage bus, and i_{rq} q-axis rotor currents of DFIG [30].

4. ESSs

The real power provided by ESS-based damping control nodes considers a promising strategy to mitigate LFO oscillations. ESS contributes to effective solutions for enhancing the quality and efficiency of power and trustworthiness issues in power systems, including power grids with multiple penetrations of renewable energy. The ESSs are also playing a pivot role for different systems. For instance, shipboard, aircraft, powertrains, electric vehicles, and power systems meet the peak load economically and enhance the reliability of the system [31]. In terms of power capabilities and run time, ESS can be divided into two primary categories: high extended /energy discharge and high rapid /power discharge [29]. Figure 6 presents a different type of ESS that is used in the power system application.

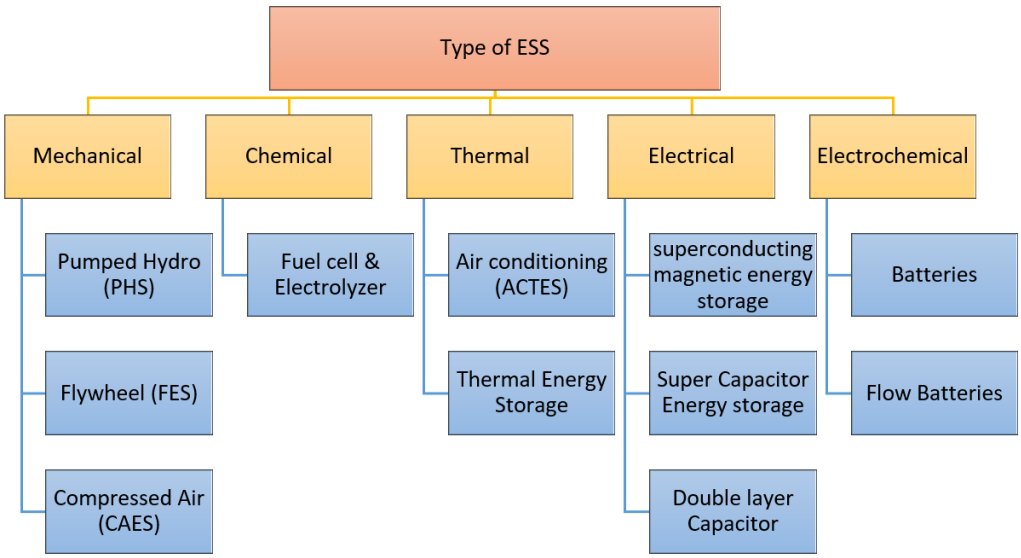

Figure 6. Type of ESS.

SMES

SMES system can store huge amounts of power in a magnetic field produced by direct current in the coil within a very short and fast response time and cooled by cryogenic [32].

That would make SMES able to inject or absorb massive amounts of energy in a very short time. Many other advantages have attracted the interest of researchers to use SMES systems to enhance power system dynamic stability. For instance, high efficiency, long lifetime, recharging of SMES can be done in just a couple of minutes and can repeat the charge and discharge modes thousands of times without reducing the magnet. Recharging time can be accelerated to meet specific criteria based on the system's capacity [33]. The main components in SMES are two parts: (1) the superconducting coil and (2) the power conversion system—consisting of inverter/rectifier circuits [26]. All previous details of SMES are shown in Figures 7 and 8. SMES can be installed at a terminal bus of the power system. The mathematical representation of SMES unit can be expressed using Equations:

$$\Delta E_d = \frac{1}{st_{dc}+1}[C_0\Delta\omega_n - C_{Id}\Delta I_d] \tag{13}$$

$$\Delta I_d = \frac{1}{Ls}\Delta E_d \tag{14}$$

where ΔI_d is the current flowing through the coil, ΔE_d is the terminal voltage applied to the coil. The K_0, and K_{ID} are constants gain and the feedback gain, respectively. $\Delta\omega_n$ represent the rotor speed deviation of the generator n [24].

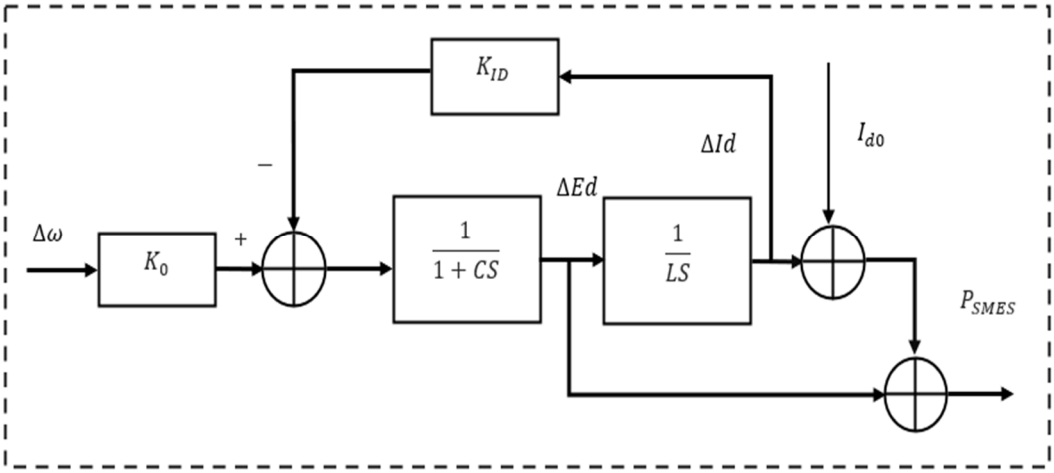

Figure 7. SMES model.

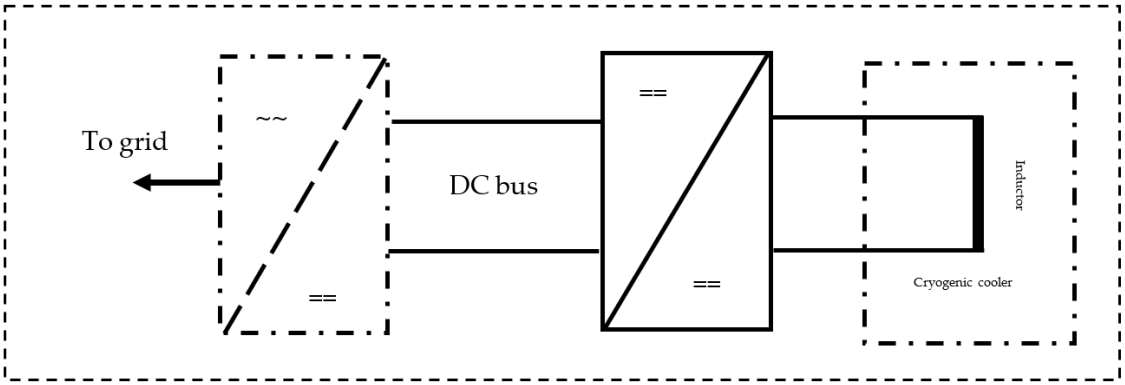

Figure 8. SMES block digram.

The active power that producing by SMES can be represented as the following equation:

$$\Delta P_{SMES} = \Delta E_d(\Delta I_{d0} + \Delta I_d) \tag{15}$$

5. PID and FOPID

The FO system is a dynamical system modeled by a fractional differential equation containing derivatives of non-integer order, as shown in Figure 9 [34]. The main feature that made this controller so popular is that we can control the fraction power to add the derivative or integral as needed. The main feature of FO is that we can control the integration/derivative and integration-derivative order to get the system's best performance. The general form of FO

$$aD_t^{\alpha} = \begin{cases} \frac{d^{\alpha}}{dt^{\alpha}} & \alpha > 0, \\ 1 & \alpha = 0, \\ \int_a^t (d\tau)^{-\alpha} & \alpha < 0, \end{cases} \tag{16}$$

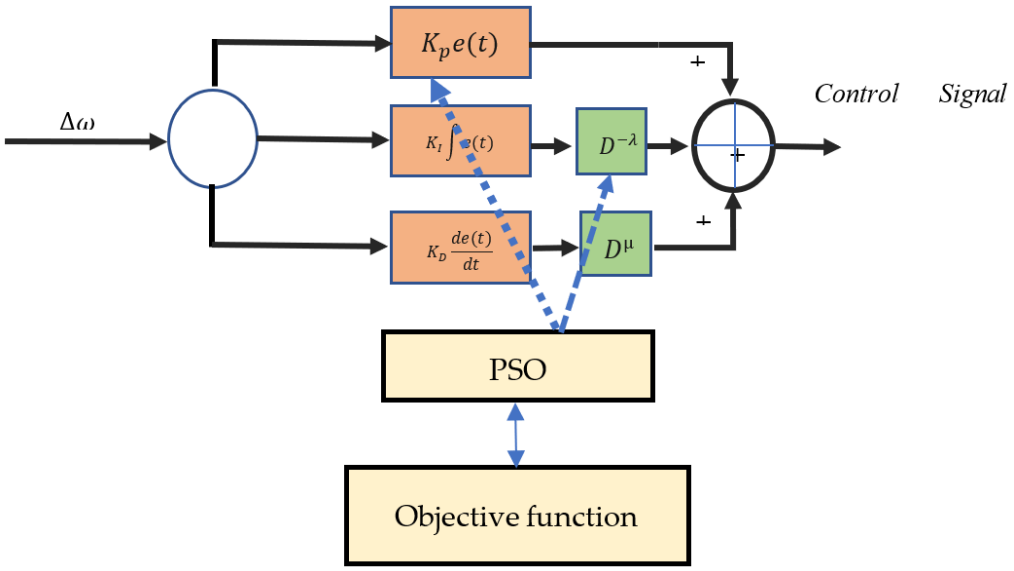

Figure 9. FOPID structure.

Here $\mu = a$ if $\alpha > 0$, $\lambda = -a$ if $\alpha < 0$ if represent the order of the differentiation or integration, respectively [33]. Table 1 provides a comparison between PID and FOPID. FO definition:

$$aD_t^{\alpha} f(t) = \frac{d^{\alpha}}{dt^{\alpha}} f(t) = \frac{1}{\Gamma(m-\alpha)dt^m} \int_{\alpha}^{t} \frac{f(\tau)}{(t-\tau)^{\alpha-m+1}} d\tau \tag{17}$$

$$aD_t^{-\alpha} f(t) = I^{\alpha} f(t) = \frac{1}{\Gamma(\alpha)} \int_{\alpha}^{\tau} \frac{f(\tau)}{(t-\tau)^{1-\alpha}} d\tau \tag{18}$$

where the $\Gamma(x)$ is calculated as the following equation:

$$\Gamma(x) = \int_0^{\infty} e^{-t} t^{(x-1)} dt, \; x > 0 \tag{19}$$

Table 1. PID and FOPID.

	PID	FOPID
Structure	Simple	Complex
No. of tuning parameters	3: *Kp*, *Ki*, *Kd*	5: *Kp*, *Ki*, *Kd*, μ, $-\lambda$
Accuracy	Low	High
Power of operation	0 or 1	Any positive integer
Effective with	Simple system	Complex system

The control single is calculated by the following Equation (20).

$$u(t) = (K_p(t) + K_D D_t^{\mu} + K_I D_t^{-\lambda})\Delta\omega \quad (20)$$

6. PSO

PSO is used to give optimum values for PID and FOPID parameters. PSO is considered an evolutionary computational algorithm that searches for a problem by iteratively improving a candidate solution concerning a given quality measure [3]. The concept of PSO is constricting several swarm particles and adjusting the fitness, as illustrated in Figure 10. The objective function F can be written as the following equation:

$$F = \int_0^T t(\Delta\omega_n)dt \quad (21)$$

where $\Delta\omega_n$ represents the rotor speed deviation for the n generator. The constraints of PSO parameters tuning are written as follows:
Minimize of F
Subject to

$$\begin{cases} K_{Pmin} \le K_P \le K_{Pmax} \\ K_{Dmin} \le K_D \le K_{Dmax} \\ K_{Imin} \le K_I \le K_{Imax} \\ \mu_{min} \le \mu \le \mu_{max} \\ \lambda_{min} \le \lambda \le \lambda_{max} \end{cases}$$

The range of PID parameters are between [0.1–50]. The values of FO μ and λ are between [0.0001–1] [17].

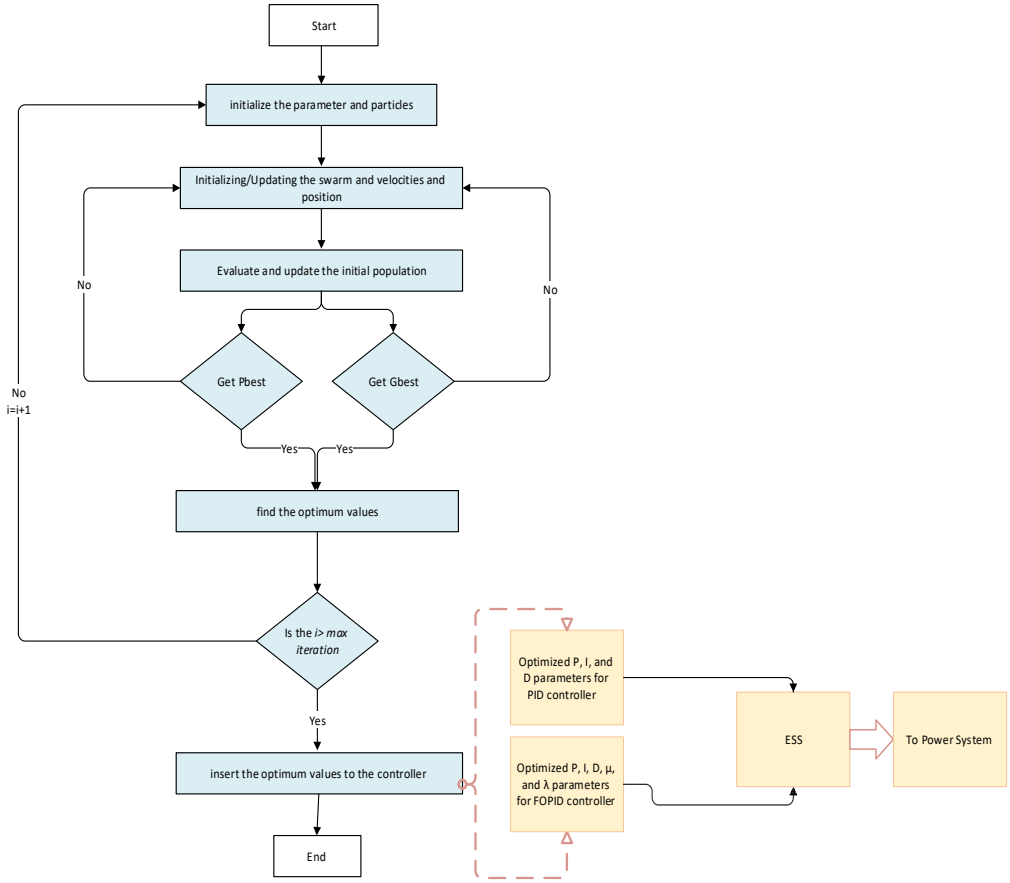

Figure 10. PSO flow chart.

7. Case Study

To investigate the contribution of ESS for damping LFO in the power system with a high level of RES is considered in this part. The multimachine power system was selected as a test model. The multimachine power system combines two areas with 12 buses and 4 synchronous generators linked by a double 220 km transmission line. There are two synchronous generators in each area with 900 MVA rated popularly known as "Kundur" power system [21]. Each area has two tightly similar units of synchronous generators. The rate for the individual unit is 20 kV and 60 Hz. An adjustment was made to the base power system by reducing the power rating of generator number 2 in area 1. Based on this work [8], the RESs have been placed at bus number 2, as illustrated in Figure 11. The compensation was produced by adding RES, as illustrated in different scenarios. To examine the contribution of SMES with the proposed controller, three different scenarios will be considered.

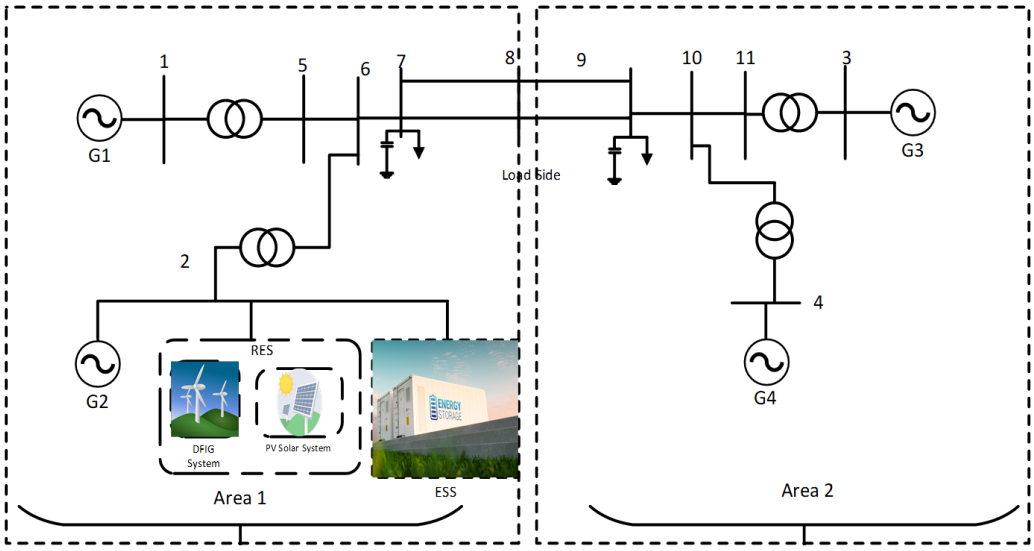

Figure 11. Proposed model.

There are three different cases in each scenario, as shown in Figure 12. In the first scenario, the power system is connected with a PV system in three different cases: (1) The power system is integrated with wind and SMES. (2) The power system is integrated with the wind system SMES and PID controller. (3) The power system is integrated with wind system SMES and FOPID controller.

In the second scenario, the power system connects to the PV system in three different cases. (1) The power system is integrated with PV and SMES. (2) The power system is integrated with PV, SMES, and PID controller. (3) The power system is integrated with PV, SMES, and FOPID controller.

n the third scenario the power system connects with the PV system and wind turbine system in three different cases. (1) The power system is integrated with PV system-wind and SMES. (2) The power system is integrated with PV system-wind SMES and PID controller. (3) The power system is integrated with PV system-wind SMES and FOPID controller. The RES will share 400 MW with generator 2 at bus number 2. The wind turbine will share 300 MW, and the PV system will share 100 MW. The SMES rating power is 10 MW. The proposed controller is installed with SMES, as shown in Figure 13.

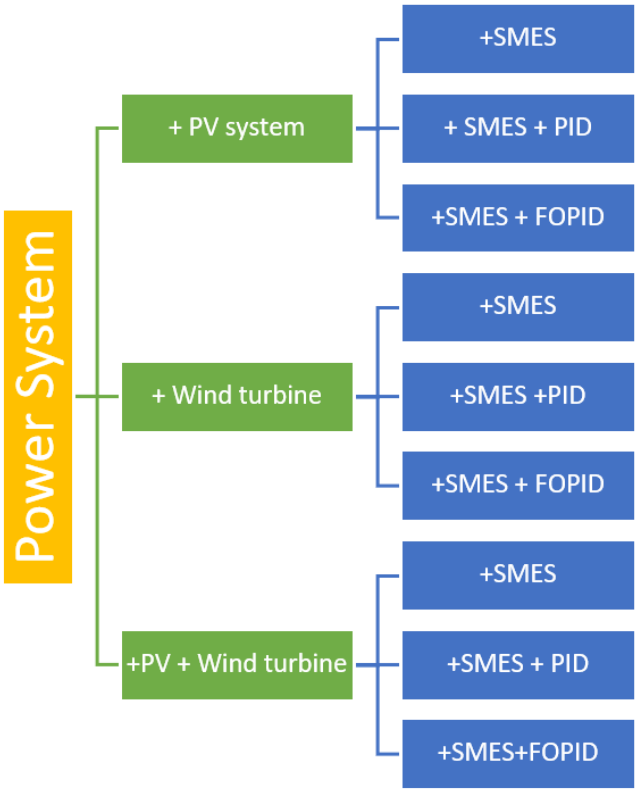

Figure 12. Investigated scenarios.

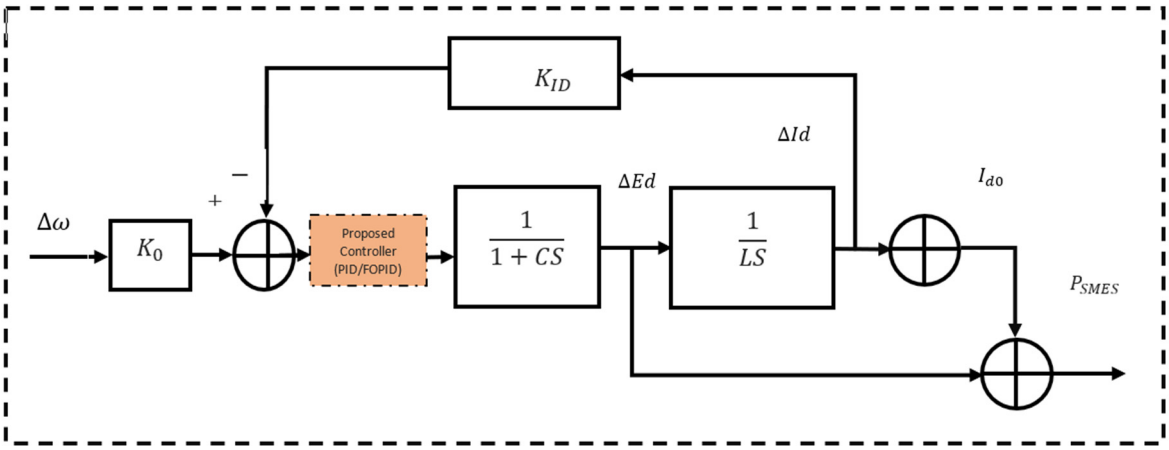

Figure 13. SMES with the proposed controllers.

Two assumptions will be considered with RES: (1) a white noise is added to the wind and PV system model to reflect the realistic power output of fluctuating profile. (2) The wind turbine and PV system are working at the maximum power point condition—the simulation results in time-domain and eigenvalues analysis.

8. Simulation Results

The previous scenarios and cases will be investigated in this part. Using PSO will obtain the optimal values for PID and FOPID parameters. The convergence PSO curves of the objective function during iteration is shown in Figure 14.

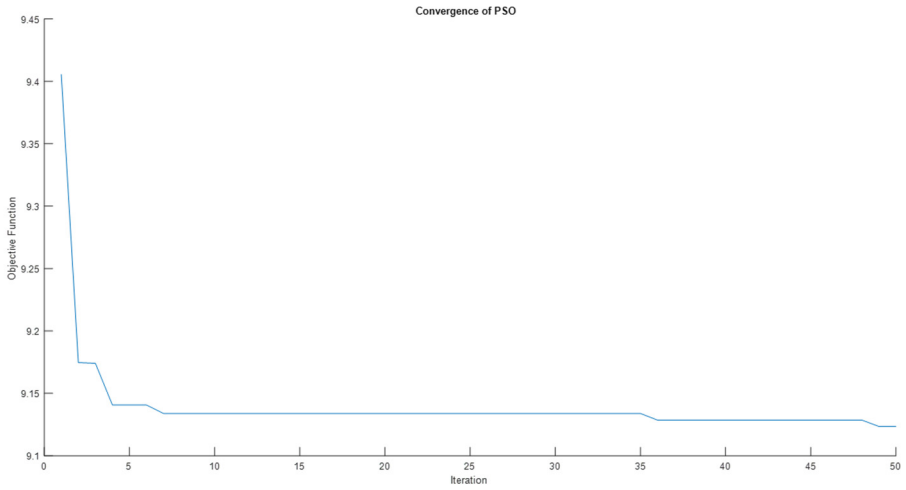

Figure 14. Convergence PSO curves.

The PSO parameters and optimized values are given in Tables 2 and 3.

Table 2. PSO parameters.

PSO Parameters	Value
Size of the swarm	50
Maximum steps	50
PSO momentum	0.9
PSO parameter C1	1.2
PSO parameter C2	0.12

Table 3. PSO optimized values.

Optimized Value	
Parameter	**Optimized Value**
K_p	0.63
K_I	0.05303
K_D	1.9688
λ	0.73
μ	0.92

The primary function of the PSO in this work is to help the controller to obtain the best values for PID and FOPID [35–37]. Therefore, when we are looking at the value of the K_D we observe that it is the larger value compared with K_p and K_I. That refers to the derivative function to reduce the overshoot in the signal. The following simulation results show the time-domain system response in different cases.

8.1. Time-Domain Simulation Results

8.1.1. Power System with Wind Turbine Scenario

The first scenario presented is (1) the power system integrated with the wind system and SMES. (2) The power system is integrated with wind system SMES and PID controller. (3) The power system is integrated with wind system SMES and FOPID controller. The wind turbine will share 300 MW at bus 2 shared with generator number 2. Figure 15 shows the rotor speed deviation. We can observe that the wind generator notably contributed to the increase in oscillation and affected the system stability. There was no significant change when the SMES were added at bus 2. In comparison, we note that when PID and FOPID were added, the system response reached stability and eliminated the oscillations.

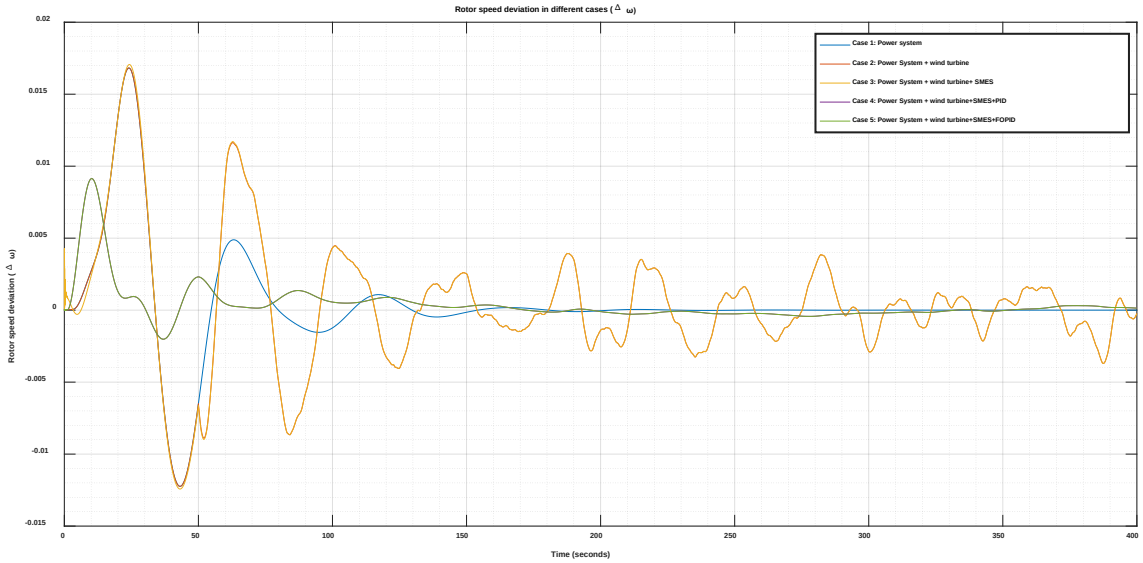

Figure 15. Rotor speed deviation in wind Turbine scenario.

The power flow in different cases is presented in Figure 16. The fluctuations caused by the wind turbine affected the stability of the power flow. It clearly shows how the FOPID controller has contributed to improving the role of SMES in mitigating LFO.

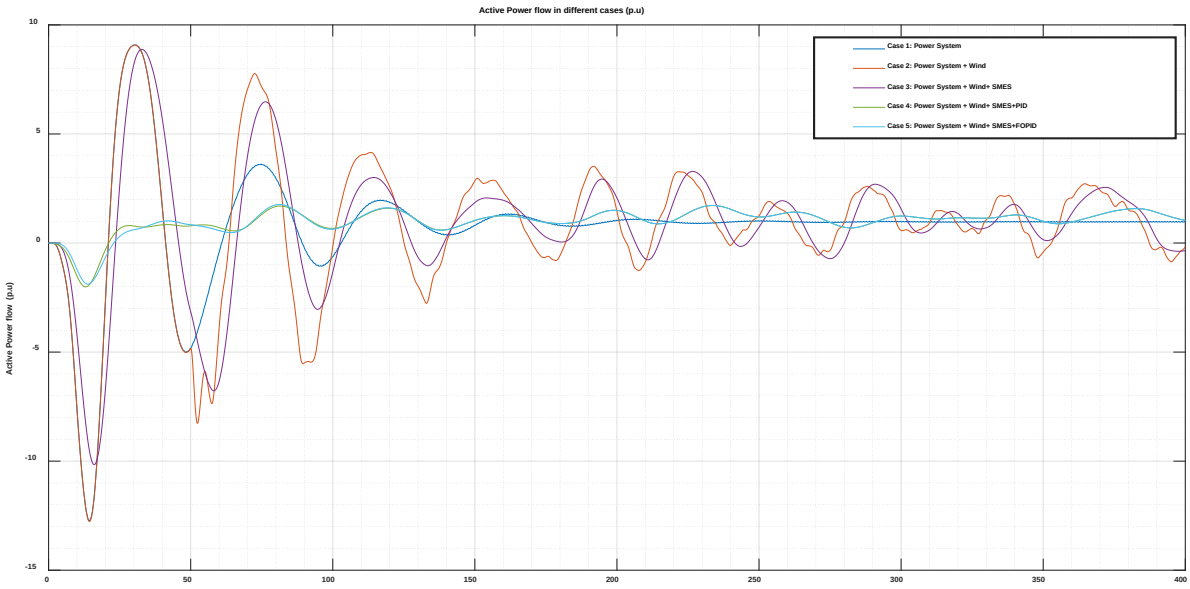

Figure 16. Active power flow in wind turbine scenario.

8.1.2. Power System with PV Scenario

The power system connects to the PV system in three different cases in the second scenario. (1) The power system is integrated with PV and SMES. (2) The power system is integrated with PV, SMES, and PID controller. (3) The power system is integrated with PV, SMES, and FOPID controller. PV system will share 100 MW. While the contribution of PV is less than the wind turbine, we can observe that the oscillation of rotor speed deviation is less than the oscillations in the wind turbine case. However, the contribution of SMES with PV is still limited. When PID has been added to SMES, it is worked to enhance the reduction of the oscillations but could not eliminate it. The FOPID, when added to SMES has excellent performance compared with PID, as shown in Figure 17.

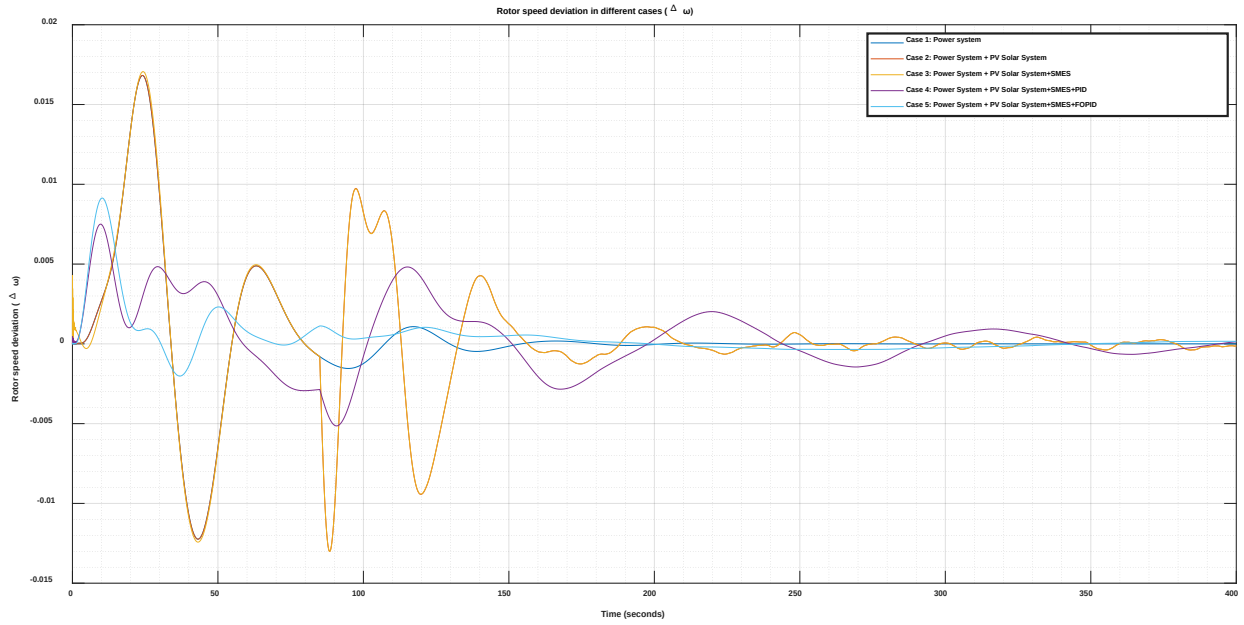

Figure 17. Rotor speed deviation in PV scenario.

The power flow in different cases is presented in Figure 18. The fluctuations caused by the PV affected the stability of the power flow. It clearly shows how the FOPID controller has contributed to improving the role of SMES in mitigating of power flow.

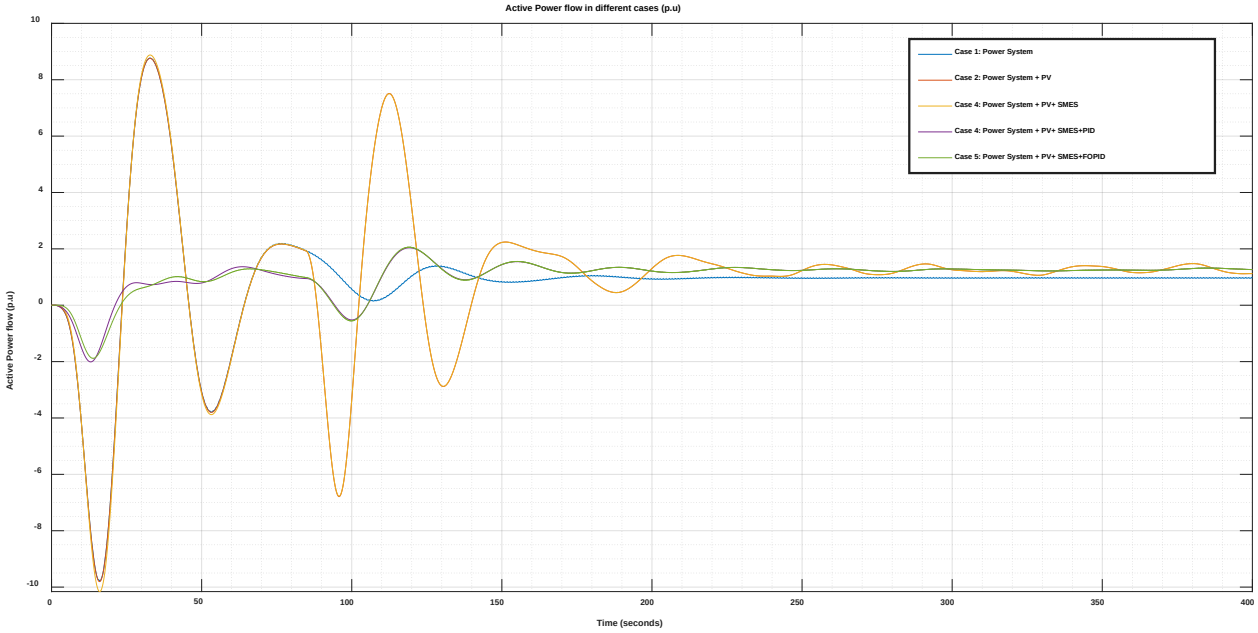

Figure 18. Active power flow in PV scenario.

8.1.3. Power System with PV and Wind Turbine Scenario

In the third scenario, the power system connects to the PV system and wind turbinein in three different cases. (1) The power system is integrated with PV system-wind and SMES. (2) The power system is integrated with PV system-wind SMES and PID controller. (3) the power system integrated with PV system-wind SMES and FOPID controller. PV system will share 100 MW, and wid turbine will share 300 MW.

We can observe that the oscillation of rotor speed deviation in this scenario is greater than in the previous cases. The FOPID supports the SMES to improve the LFO, as shown in Figure 19.

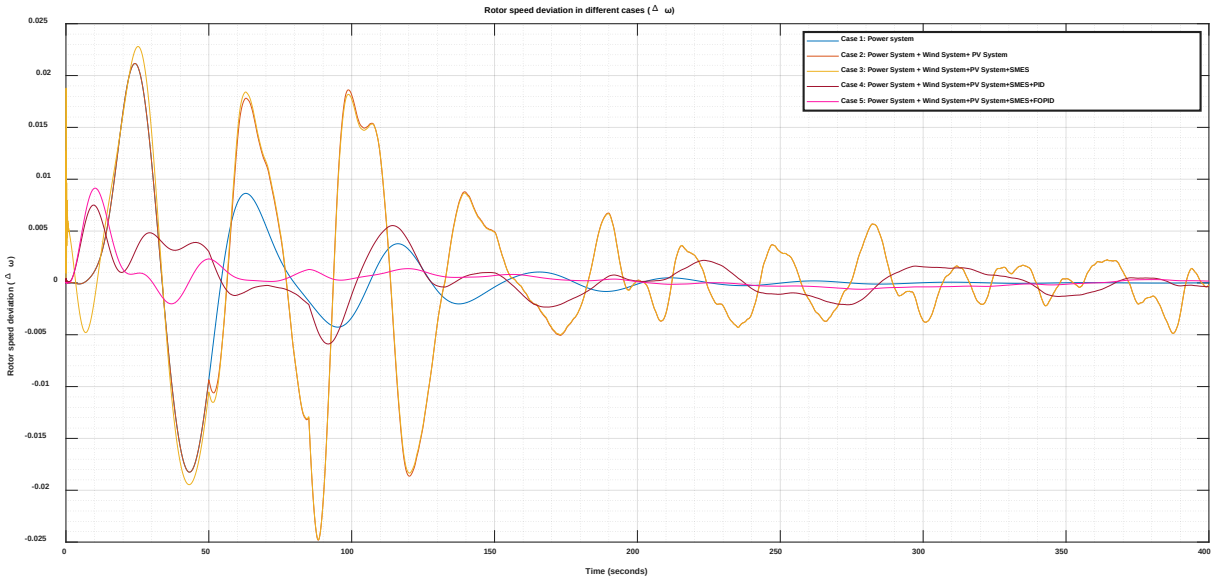

Figure 19. Rotor speed deviation in PV and wind turbine scenario.

The power flow in different cases is presented in Figure 20. The fluctuations caused by the PV and wind systems affected the stability of the power flow. It clearly shows how the FOPID controller has contributed to improving the role of SMES in mitigating power flow.

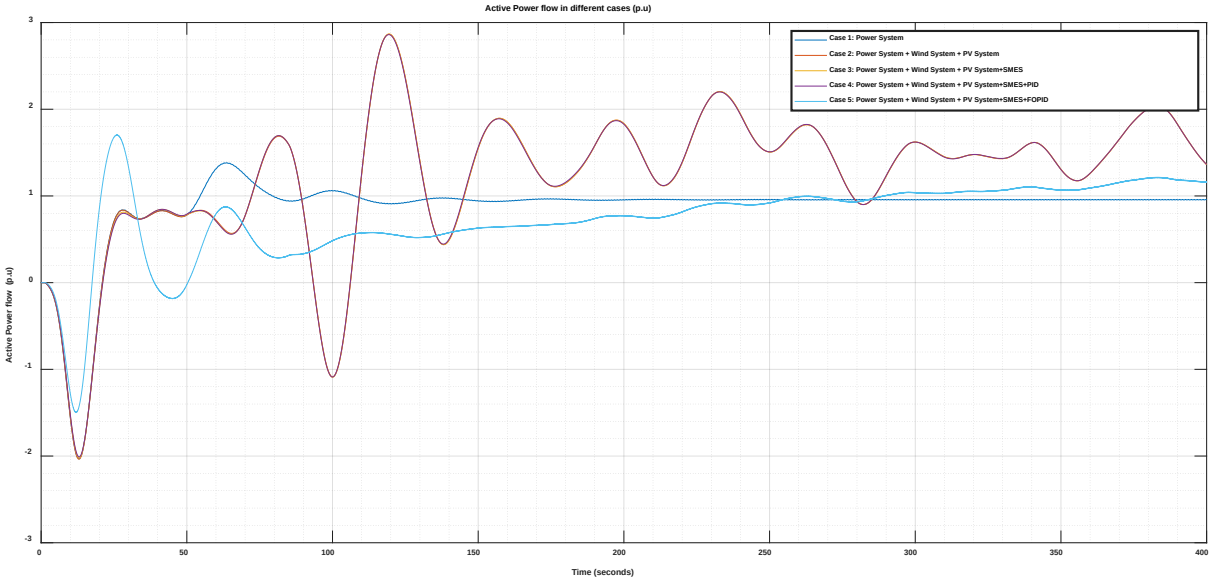

Figure 20. Active power flow in PV and wind scenario.

Table 4 shows an explicit comparison between the proposed controllers with other handled cases in the context.

Table 4. Comparison of overshoot (OS) and settling time (ST) in different cases.

Scenario #	Cases	Δw		P	
		OS	ST (s)	OS	ST (s)
Scenario 1	Power System + PV	0.118	-	0.255	-
	Power System + PV + SMES	0.116	55	0.243	-
	Power System + PV + SMES + PID	0.058	35	0.053	20
	Power System + PV + SMES + FOPID	0.0608	15	0.033	13
Scenario 2	Power System + Wind	0.119	-	0.355	-
	Power System + Wind + SMES	0.115	50	0.341	-
	Power System + Wind + SMES + PID	0.0707	20	0.051	25
	Power System + Wind + SMES + FOPID	0.066	10	0.032	11
Scenario 3	Power System + Wind + PV	0.1192	-	0.345	-
	Power System +PV+ Wind + SMES	0.1177	60	0.333	-
	Power System + PV+ Wind + SMES + PID	0.0911	25	0.025	28
	Power System + PV + Wind + SMES + FOPID	0.0902	10	0.022	10

The above table compares the values of the settling time and overshoot of the dynamic performance of the rotor speed divination and active power flow in each case. In all cases, the proposed controller enhances the rotor speed divination and active power flow response and conveys them to zero in the steady-state.

To prove the superiority of the FOPID, Table 5 compares different errors criteria such as the integral time-squared error (ITSE), Integral time absolute error (ITAE), the integral absolute error (IAE), and integral squared error (ISE) [38].

Table 5. Errors comparison in different cases.

	Error Criteria			
Cases 1	ISE	ITSE	IAE	ITAE
Power System + PV + SMES + PID	0.0000742	0.0000712	0.2203	1.982
Power System + PV + SMES + FOPID	0.0000954	0.0000559	0.2037	1.843
Cases 2	ISE	ITSE	IAE	ITAE
Power System + Wind + SMES + PID	0.00000533	0.0004233	0.2223	2.223
Power System + Wind + SMES + FOPID	0.00000512	0.0000411	0.2038	2.038
Cases 3	ISE	ITSE	IAE	ITAE
Power System + PV + Wind + SMES + PID	0.0000155	0.0009551	0.2732	2.732
Power System + PV + Wind + SMES + FOPID	0.0000144	0.0001176	0.2552	2.552

8.2. Analysis of Eigenvalues

The Equations (22)–(24) are used to obtain the oscillation frequency and the damping ratio [7].

$$\lambda_i = \sigma_i \pm j\omega_i \tag{22}$$

$$f_i = \frac{\omega_i}{2\pi} \tag{23}$$

$$\xi(\%) = \frac{-\sigma_i}{\sqrt{-\sigma_i^2 + \omega_i^2}} \tag{24}$$

From the analysis of the eigenvalues, we can observe that there is one inter-area oscillation and two local-area oscillations for each case. Also, we can observe that the LFO in cases that RES shared their power capacity to the power system increased due to adding RES (PV, wind, PV, and wind), and the damping of LFO decreased.

Adding SMES is still limited on the LFO and the damping ratio with RES. However, the effect of SMES with PID and FOPID appears to decrease in LFO and enhance the damping ratio in the power system with RES context, as shown in Figures 21 and 22.

Moreover, the effect of FOPID with SMES is considered acceptable despite not eliminating the oscillations definitively.

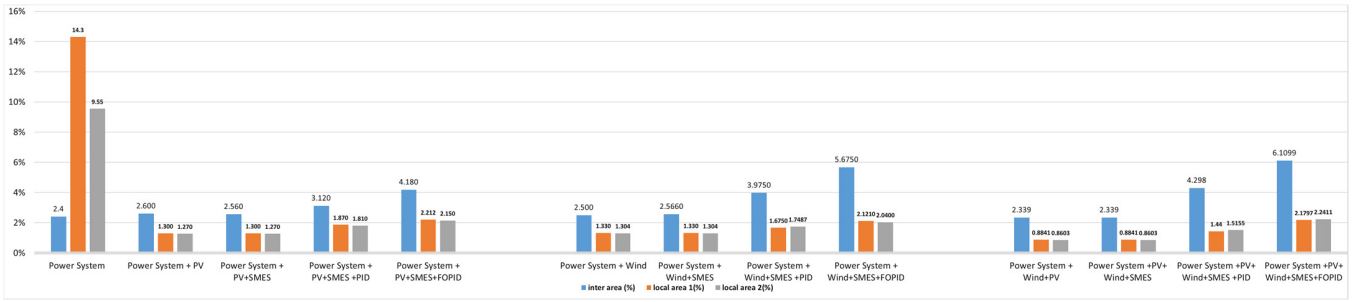

Figure 21. Damping oscillation in different cases.

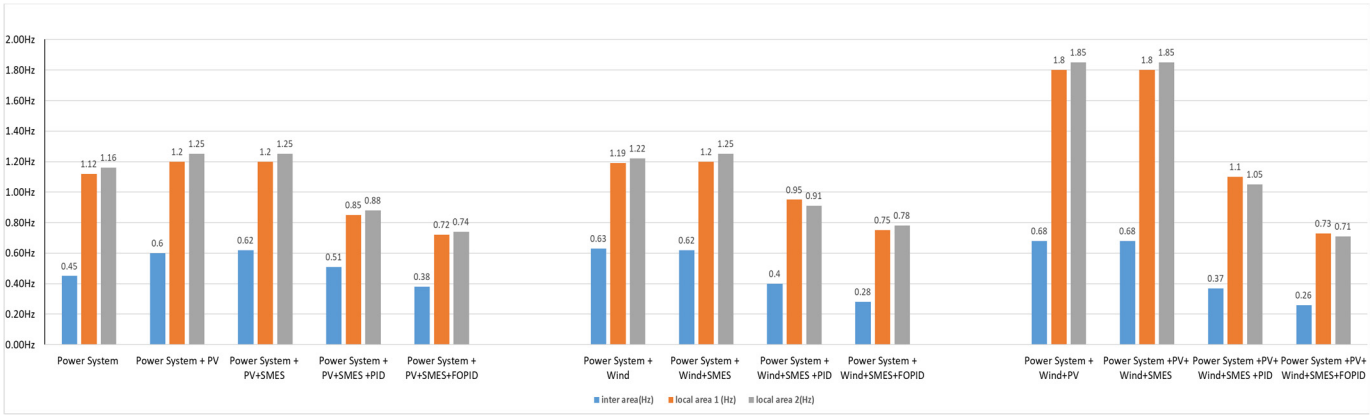

Figure 22. Frequency oscillation in different cases.

9. Conclusions

This study presented the effect of adding renewable energy sources such as wind and PV systems with high penetration in the multimachine power system. It also studied the effect of adding SMES as an ESS proposed in different cases such as merging PV system only, merging wind energy only, and merging PV solar system and wind turbine. The results showed that adding RES negatively affects the system's stability by reducing the damping coefficient and increasing the low-frequency oscillation in the power system. The PID and FOPID controllers, which were proposed to be added with SMES, played a pivot role in improving the damping low-frequency oscillation, improving the power system stability, and allowing for high penetration of RES. The PSO proposed method for selecting the optimum parameters for the PID and FOPID also showed a high performance that contributed to effective damping of the oscillation that arises through the integration of renewable energy sources. The simulation results in time-domain and eigenvalues analysis confirm that the FOPID controller based on the SMES enhanced the damping LFO in the multimachine power system with RES context better than the PID controller. Thus, the ESS can play an important role in improving the stability of the power systems integrated with high penetration of RES. Further research is required to utilize advanced and robust control methods to avoid potential interactions, avoid the unstable operating condition of power systems, and fast up to obtain optimal operating conditions for power systems within the RES context.

Author Contributions: Conceptualization, H.A.A., Funding acquisition, H.A.A.; Investigation, H.A.A.; Methodology, H.A.A.; Software, H.A.A.; Supervision, A.M.V.; Writing—original draft, H.A.A.; Writing—review & editing, A.M.V. All authors have read and agreed to the published version of the manuscript.

Funding: This work received no external funding.

Conflicts of Interest: The authors declare no conflict of interest.

References

1. Masson-Delmotte, V.; Zhai, P.; Chen, Y.; Goldfarb, L.; Gomis, M.I.; Matthews, J.B.R.; Berger, S.; Huang, M.; Yelekçi, O.; Yu, R.; et al. *Working Group I Contribution to the Sixth Assessment Report of the Intergovernmental Panel on Climate Change*; IPCC: Geneva, Switzerland, 2021; ISBN 9789291691586.
2. Energy Agency, I. *Renewables 2021—Analysis and Forecast to 2026*; International Energy Agency: Paris, France, 2021.
3. Shafiul Alam, M.; Al-Ismail, F.S.; Salem, A.; Abido, M.A. High-Level Penetration of Renewable Energy Sources into Grid Utility: Challenges and Solutions. *IEEE Access* **2020**, *8*, 190277–190299. [CrossRef]
4. Impram, S.; Varbak Nese, S.; Oral, B. Challenges of Renewable Energy Penetration on Power System Flexibility: A Survey. *Energy Strategy Rev.* **2020**, *31*, 100539. [CrossRef]
5. Kundur, P.; Paserba, J.; Ajjarapu, V.; Andersson, G.; Bose, A.; Canizares, C.; Hatziargyriou, N.; Hill, D.; Stankovic, A.; Taylor, C.; et al. Definition and Classification of Power System Stability. *IEEE Trans. Power Syst.* **2004**, *19*, 1387–1401. [CrossRef]
6. Shah, R.; Mithulananthan, N.; Bansal, R.C. Damping Performance Analysis of Battery Energy Storage System, Ultracapacitor and Shunt Capacitor with Large-Scale Photovoltaic Plants. *Appl. Energy* **2012**, *96*, 235–244. [CrossRef]
7. Vural, A.M. Contribution of High Voltage Direct Current Transmission Systems to Inter-Area Oscillation Damping: A Review. *Renew. Sustain. Energy Rev.* **2016**, *57*, 892–915. [CrossRef]
8. Abumeteir, H.A.; Vural, A.M. Impact of High Penetration Renewable Energy Systems on Low-Frequency Oscillations. In Proceedings of the 2021 International Conference on Electric Power Engineering–Palestine (ICEPE-P), Gaza, Palestine, 23–24 March 2021; IEEE: Piscataway, NJ, USA, 2021; pp. 1–4.
9. Sui, X.; Tang, Y.; He, H.; Wen, J. Energy-Storage-Based Low-Frequency Oscillation Damping Control Using Particle Swarm Optimization and Heuristic Dynamic Programming. *IEEE Trans. Power Syst.* **2014**, *29*, 2539–2548. [CrossRef]
10. Setiadi, H.; Krismanto, A.U.; Mithulananthan, N.; Hossain, M.J. Modal Interaction of Power Systems with High Penetration of Renewable Energy and BES Systems. *Int. J. Electr. Power Energy Syst.* **2018**, *97*, 385–395. [CrossRef]
11. Beza, M.; Bongiorno, M. An Adaptive Power Oscillation Damping Controller by STATCOM with Energy Storage. *IEEE Trans. Power Syst.* **2015**, *30*, 484–493. [CrossRef]
12. Zhu, Y.; Liu, C.; Wang, B.; Sun, K. Damping Control for a Target Oscillation Mode Using Battery Energy Storage. *J. Mod. Power Syst. Clean Energy* **2018**, *6*, 833–845. [CrossRef]
13. Datta, U.; Kalam, A.; Shi, J. Battery Energy Storage System Control for Mitigating PV Penetration Impact on Primary Frequency Control and State-of-Charge Recovery. *IEEE Trans. Sustain. Energy* **2020**, *11*, 746–757. [CrossRef]
14. Setiadi, H.; Mithulananthan, N.; Shah, R. Design of Wide-Area POD with Resiliency Using Modified DEA for Power Systems with High Penetration of Renewable Energy. *IET Renew. Power Gener.* **2019**, *13*, 342–351. [CrossRef]
15. Setiadi, H.; Mithulananthan, N.; Shah, R.; Lee, K.Y.; Krismanto, A.U. Resilient Wide-Area Multi-Mode Controller Design Based on Bat Algorithm for Power Systems with Renewable Power Generation and Battery Energy Storage Systems. *IET Gener. Transm. Distrib.* **2019**, *13*, 1884–1894. [CrossRef]
16. Ma, J.; Wang, T.; Thorp, J.S.; Wang, Z.; Yang, Q.; Phadke, A.G. WAMS Based Damping Control of Inter-Area Oscillations Employing Energy Storage System. *Adv. Electr. Comput. Eng.* **2012**, *12*, 33–40. [CrossRef]
17. Neely, J.C.; Byrne, R.H.; Elliott, R.T.; Silva-Monroy, C.A.; Schoenwald, D.A.; Trudnowski, D.J.; Donnelly, M.K. Damping of Inter-Area Oscillations Using Energy Storage. In Proceedings of the 2013 IEEE Power & Energy Society General Meeting, Vancouver, BC, Canada, 21–25 July 2013. [CrossRef]
18. Bamasak, S.M.; Kumar, S.R.; Al-Turki, Y.A. Design of Wide Area Fractional-Order PID Damping Controller for Inter-Area Low-Frequency Oscillations Using Differential Evolution. *J. Eng. Res.* **2018**, *6*, 94–115.
19. He, T.; Li, S.; Wu, S.; Li, K. Small-Signal Stability Analysis for Power System Frequency Regulation with Renewable Energy Participation. *Math. Probl. Eng.* **2021**, *2021*, 5556062. [CrossRef]
20. Zhu, Y.; Liu, C.; Sun, K.; Shi, D.; Wang, Z. Optimization of Battery Energy Storage to Improve Power System Oscillation Damping. *IEEE Trans. Sustain. Energy* **2019**, *10*, 1015–1024. [CrossRef]
21. Darvish Falehi, A. Optimal Robust Disturbance Observer Based Sliding Mode Controller Using Multi-Objective Grasshopper Optimization Algorithm to Enhance Power System Stability. *J. Ambient Intell. Humaniz. Comput.* **2020**, *11*, 5045–5063. [CrossRef]
22. Kundur, P. *Power System Stability and Control—McGraw-Hill Education*; McGraw Hill: New York, NY, USA, 1994; ISBN 007035958X.
23. Darvish Falehi, A. Optimal Fractional Order BELBIC to Ameliorate Small Signal Stability of Interconnected Hybrid Power System. *Environ. Prog. Sustain. Energy* **2019**, *38*, 13208. [CrossRef]
24. Panda, S. Differential Evolutionary Algorithm for TCSC-Based Controller Design. *Simul. Model. Pract. Theory* **2009**, *17*, 1618–1634. [CrossRef]
25. Lastomo, D.; Setiadi, H.; Djalal, M.R. Optimization of SMES and TCSC Using Particle Swarm Optimization for Oscillation Mitigation in a Multi Machines Power System. *J. Mechatron. Electr. Power Veh. Technol.* **2017**, *8*, 11–21. [CrossRef]

26. Elmelegi, A.; Mohamed, E.A.; Aly, M.; Ahmed, E.M.; Mohamed, A.A.A.; Elbaksawi, O. Optimized Tilt Fractional Order Cooperative Controllers for Preserving Frequency Stability in Renewable Energy-Based Power Systems. *IEEE Access* **2021**, *9*, 8261–8277. [CrossRef]
27. Alam, M.S.; Alotaibi, M.A.; Alam, M.A.; Hossain, M.A.; Shafiullah, M.; Al-Ismail, F.S.; Rashid, M.M.U.; Abido, M.A. High-Level Renewable Energy Integrated System Frequency Control with Smes-Based Optimized Fractional Order Controller. *Electronics* **2021**, *10*, 511. [CrossRef]
28. Mohamed, E.A.; Ahmed, E.M.; Elmelegi, A.; Aly, M.; Elbaksawi, O.; Mohamed, A.A.A. An Optimized Hybrid Fractional Order Controller for Frequency Regulation in Multi-Area Power Systems. *IEEE Access* **2020**, *8*, 213899–213915. [CrossRef]
29. Vigya; Mahto, T.; Malik, H.; Mukherjee, V.; Alotaibi, M.A.; Almutairi, A. Renewable Generation Based Hybrid Power System Control Using Fractional Order-Fuzzy Controller. *Energy Rep.* **2021**, *7*, 641–653. [CrossRef]
30. Gupta, A.K.; Verma, K.; Niazi, K.R. Dynamic Impact Analysis of DFIG-Based Wind Turbine Generators on Low-Frequency Oscillations in Power System. *IET Gener. Transm. Distrib.* **2017**, *11*, 4500–4510. [CrossRef]
31. Farhadi, M.; Mohammed, O. Energy Storage Technologies for High-Power Applications. *IEEE Trans. Ind. Appl.* **2016**, *52*, 1953–1962. [CrossRef]
32. Setiadi, H.; Robandi, I.; Yuwono, T. Penalaan Parameter Superconducting Magnetic Energy Storage (SMES) Menggunakan Firefly Algorithm (FA) Pada Sistem Tenaga Listrik Multimesin. *J. Tek. ITS* **2014**, *3*, B12–B17. [CrossRef]
33. Díaz-González, F.; Sumper, A.; Gomis-Bellmunt, O. *Energy Storage in Power Systems*; John Wiley & Sons: Hoboken, NJ, USA, 2016; ISBN 1118971329.
34. Mchiri, L.; ben Makhlouf, A.; Baleanu, D.; Rhaima, M. Finite-Time Stability of Linear Stochastic Fractional-Order Systems with Time Delay. *Adv. Differ. Eq.* **2021**, *2021*, 1–10. [CrossRef]
35. Latif, A.; Hussain, S.M.S.; Das, D.C.; Ustun, T.S.; Iqbal, A. A Review on Fractional Order (FO) Controllers' Optimization for Load Frequency Stabilization in Power Networks. *Energy Rep.* **2021**, *7*, 4009–4021. [CrossRef]
36. Elkasem, A.H.A.; Kamel, S.; Hassan, M.H.; Khamies, M.; Ahmed, E.M. An Eagle Strategy Arithmetic Optimization Algorithm for Frequency Stability Enhancement Considering High Renewable Power Penetration and Time-Varying Load. *Mathematics* **2022**, *10*, 854. [CrossRef]
37. Saadatmand, M.; Mozafari, B.; Gharehpetian, G.B.; Soleymani, S. Optimal PID Controller of Large-Scale PV Farms for Power Systems LFO Damping. *Int. Trans. Electr. Energy Syst.* **2020**, *30*, e12372. [CrossRef]
38. Ahmed, E.M.; Elmelegi, A.; Shawky, A.; Aly, M.; Alhosaini, W.; Mohamed, E.A. Frequency Regulation of Electric Vehicle-Penetrated Power System Using MPA-Tuned New Combined Fractional Order Controllers. *IEEE Access* **2021**, *9*, 107548–107565. [CrossRef]